Supporting Information

Iridium-doping boosting the electrochemical performance of lithium rich cathodes for Li-ion batteries

Yu Huang[a#], Kai Wu[a#], Ronghui Hao[a], Wenkang Miao[a], Yueling Cai[a], Peng Wang[a], Jipeng Cheng[c,d], Zihan Wang[a], Qianqian Li[a*], Bingkun Guo[a*], Anmin Nie[a, b*]

[a]*Materials Genome Institute, Shanghai University, Shanghai 200444, China*

[b]*Center for High Pressure Science, State Key Laboratory of Metastable Materials Science and Technology, Yanshan University, Qinhuangdao 066004, China*

[c]*Department of Materials Science and Engineering, State Key Laboratory of Silicon Materials, Zhejiang University, Hangzhou 310027, China*

[d]*School of Physics and Microelectronics, Zhengzhou University, Zhengzhou 450052, China*

[#]*These authors contributed equally to the work.*

** To whom correspondence should be addressed. E-mails: qianqianli@shu.edu.cn (Qianqian Li), guobingkun@shu.edu.cn (Bingkun Guo), and anmin@ysu.edu.cn (Anmin Nie)..*

Number of pages: 4

Number of Figures: 6

Number of Tables: 2

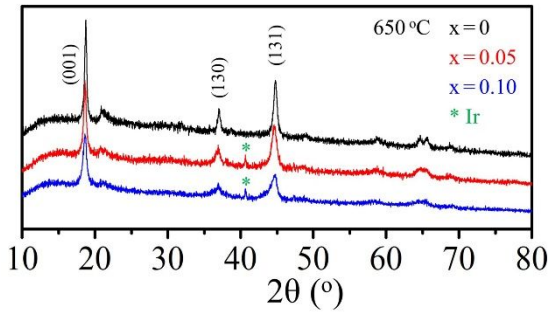

Figure S1. XRD of $Li_2(Ir_xMn_{1-x})O_3$ (x = 0, 0.05 and 0.10) powder particles at 650 °C.

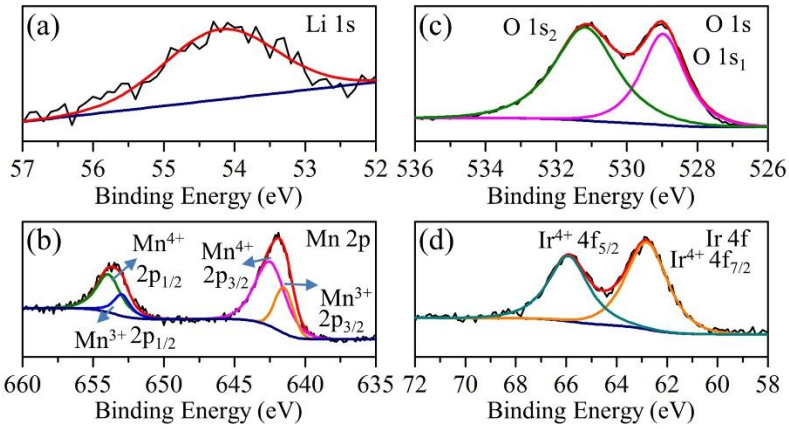

Figure S2. The XPS of $Li_2(Ir_{0.05}Mn_{0.95})O_3$-850°C sample.

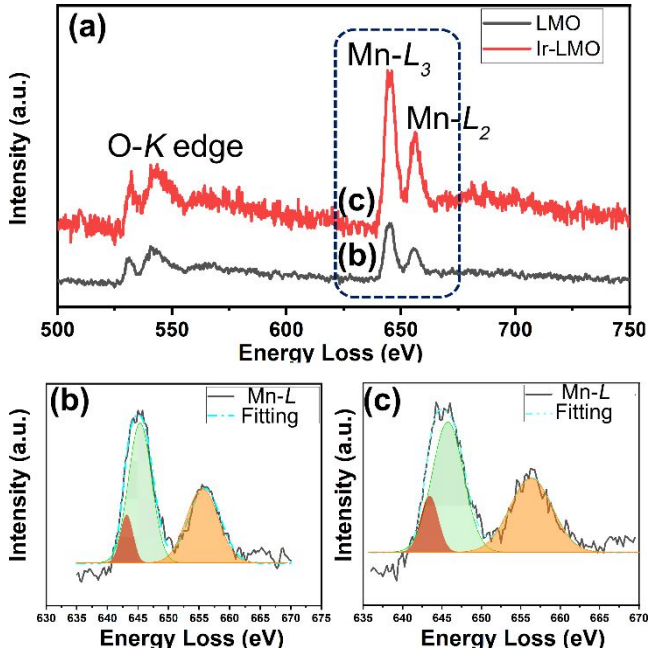

Figure S3. Electron energy loss spectroscopy (EELS) profile of the Li_2MnO_3 before and after iridium doping. (a) The typical O-K and Mn-L edge of these two specimens. (b) and (c) are the corresponding magnification of the squared region in (a).

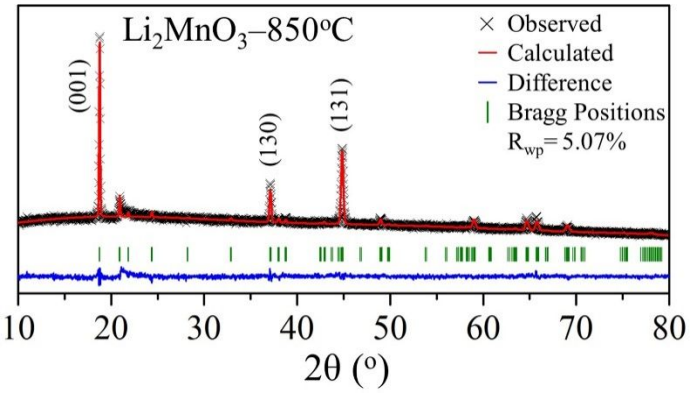

Figure S4. Powder X-ray diffraction pattern and Rietveld refinement profile of Li_2MnO_3-850°C.

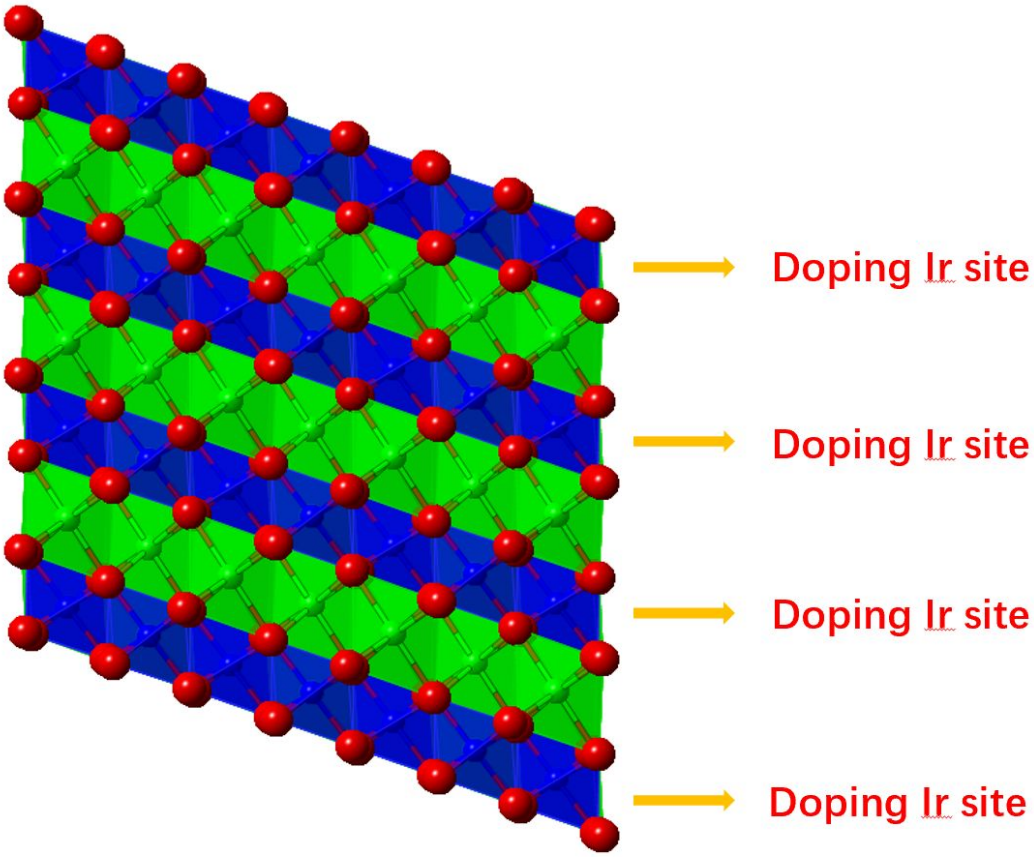

Figure S5. Schematic illustrations of crystal structures O_3-type of $Li_2(Ir_xMn_{1-x})O_3$.

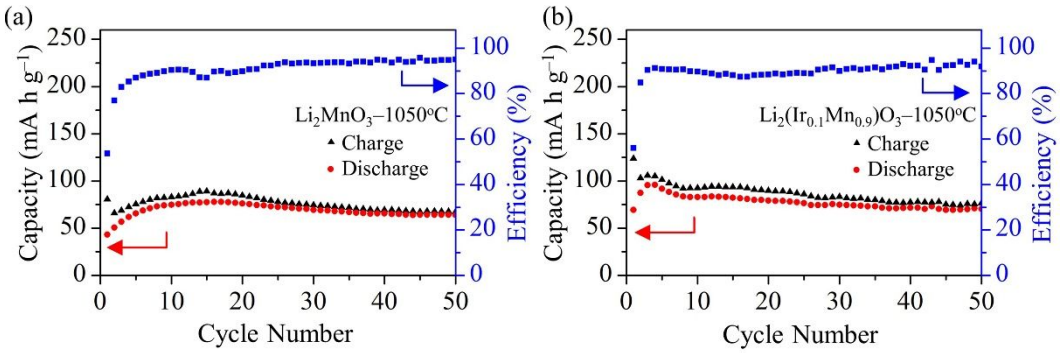

Figure S6. Cycling performances of (a) Li_2MnO_3-1050°C and (b) $Li_2(Ir_{0.1}Mn_{0.9})O_3$-1050°C in a voltage window of 2.0-4.8V.

Table S1. The values of XPS elemental peaks for Li_2MnO_3-850°C, $Li_2(Ir_{0.05}Mn_{0.95})O_3$-850°C and $Li_2(Ir_{0.1}Mn_{0.9})O_3$-850°C.

	Li_2MnO_3 –850°C	**$Li_2(Ir_{0.05}Mn_{0.95})O_3$ –850°C**	**$Li_2(Ir_{0.1}Mn_{0.9})O_3$ –850°C**
Li 1s	54.15 eV	54.21 eV	54.88 eV
O $1s_1$	529.01 eV	528.97 eV	529.10 eV
O $1s_2$	531.14 eV	531.22 eV	531.46 eV
Mn^{3+} $2p_{3/2}$	641.43 eV	641.49 eV	641.65 eV
Mn^{3+} $2p_{1/2}$	652.78 eV	652.96 eV	653.09 eV
Mn^{4+} $2p_{3/2}$	642.31 eV	642.47 eV	642.68 eV
Mn^{4+} $2p_{1/2}$	653.79 eV	653.91 eV	654.17 eV
Ir^{4+} $4f_{7/2}$		62.81 eV	63.11 eV
Ir^{4+} $4f_{5/2}$		65.91 eV	66.14 eV

Table S2. Energies (eV) of the Mn L_3 and L_2 edge peak, the integrated area ratio of L_3/L_2, and the Mn^{3+}/Mn^{4+} ratio.

Sample	L_3 main peak (eV)	L_2 main peak (eV)	I(L_3)/(L_2) ratio	Mn^{3+} main peak (eV)	Mn^{4+} main peak (eV)	I (Mn^{3+})/(Mn^{4+}) ratio
Li_2MnO_3	645.02	655.91	1.67	643.37	645.62	0.18
Ir-Li_2MnO_3	644.92	656.35	1.63	643.73	645.81	0.24